6th International Symposium on Three-Dimensional Electromagnetics
Berkeley, California, USA, March 28-30, 2017

Modelling 3D anisotropic conductivity anomalies challenging 3D isotropic inversion

Andreas Junge[1]
[1]Goethe-Universität Frankfurt am Main, Germany

SUMMARY

An anisotropic cube embedded in the subsurface gives rise to complicated patterns of the time varying electromagnetic field components of an electromagnetic wave propagating into the half space. The direction of the principal axis of the anomalous body is varied with azimuth and dip. Relations between magnetic and electric fields and current density and magnetotelluric transfer functions such as apparent resistivity, phase, tipper and phase tensor are investigated. It turns out that the electric current density is influenced strongly by charges at the boundaries of the anisotropic cube. The currents are deflected above the anomaly towards the direction of the resistive principal axis yielding a characteristic pattern of the vertical magnetic field component. The transfer functions are mainly influenced by the electric field behaviour at the surface. It is postulated that the implementation of anisotropic bodies in conductivity models might lead to geologically more reasonable conductivity models than e.g. equivalent high contrast dike structures from isotropic 3D inversion. Thus the findings provide some basics for an anticipated inversion strategy in view of 3D anisotropic conductivity anomalies.

Keywords: forward modeling, 3d anisotropy, current density distribution,

INTRODUCTION

Inverting geoelectromagnetic data observed at the Earth's surface often results in laterally alternating isotropic conductivity structures of geologically unreasonable high conductivity contrast. It turns out that in some cases these structures may be replaced by anisotropic bodies with a moderate ratio of its principal values and thus higher credibility for its interpretation (Löwer and Junge, 2016). Albeit additional parameters are introduced, the advantage of modelling intrinsic anisotropy is obvious as e.g. its simulation by a sequence of isotropic dikes with high conductivity contrast demands rather thorough numerical treatment including fine gridding and thus increasing the number of grid cells. Moreover, anisotropy of arbitrary azimuth, dip and slant will be hard to model by FD codes.

In the context of anisotropic bodies magnetotelluric transfer functions such as impedance and phase tensors as well as magnetic transfer functions like tipper and perturbation matrix reveal characteristic spatial patterns when displayed for a sequence of increasing periods. To understand the complex nature of the transfer functions it is necessary to investigate the impact of anisotropic bodies of different spatial extension and anisotropy parameters (principle values, Euler angles) on the magnetic and telluric field components separately. The propagation of the fields and the spatial distribution of the induced electrical currents and of the pointing vectors describe the induction process within the Earth. Their visual inspection compared to the observed field components at the surface reveals sensitivities and thus implies strategies for anisotropic 3D inversion schemes.

MODEL SETUP

For modelling a simple anisotropic cube was embedded in a homogeneous $100\ \Omega m$ half space (Fig. 1).

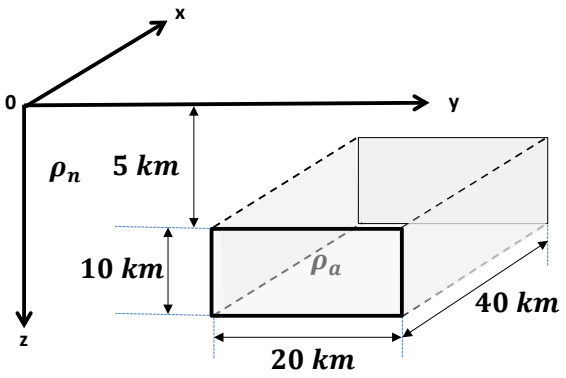

Figure 1. Model setup with background resistivity $\rho_n = 100\ \Omega m$ and embedded cube with (an)isotropic anomalous resistivity ρ_a (cf Tab. 1).

The numerical model calculations were performed with the FE software Comsol Multiphysics 5.2a™. Anticipating future inversion strategies, the resistivity distribution within the modelled volume is defined at support points distributed in a user defined spatial pattern. The resistivity values are projected on the unstructured FE grid which may vary in size according to the area of interest and the properties of the diffusing EM fields. The size of the modelled volume is of the order of several skin depths to avoid boundary effects. The average number of cells is 40,000 with ca 500.000 degrees of freedom.

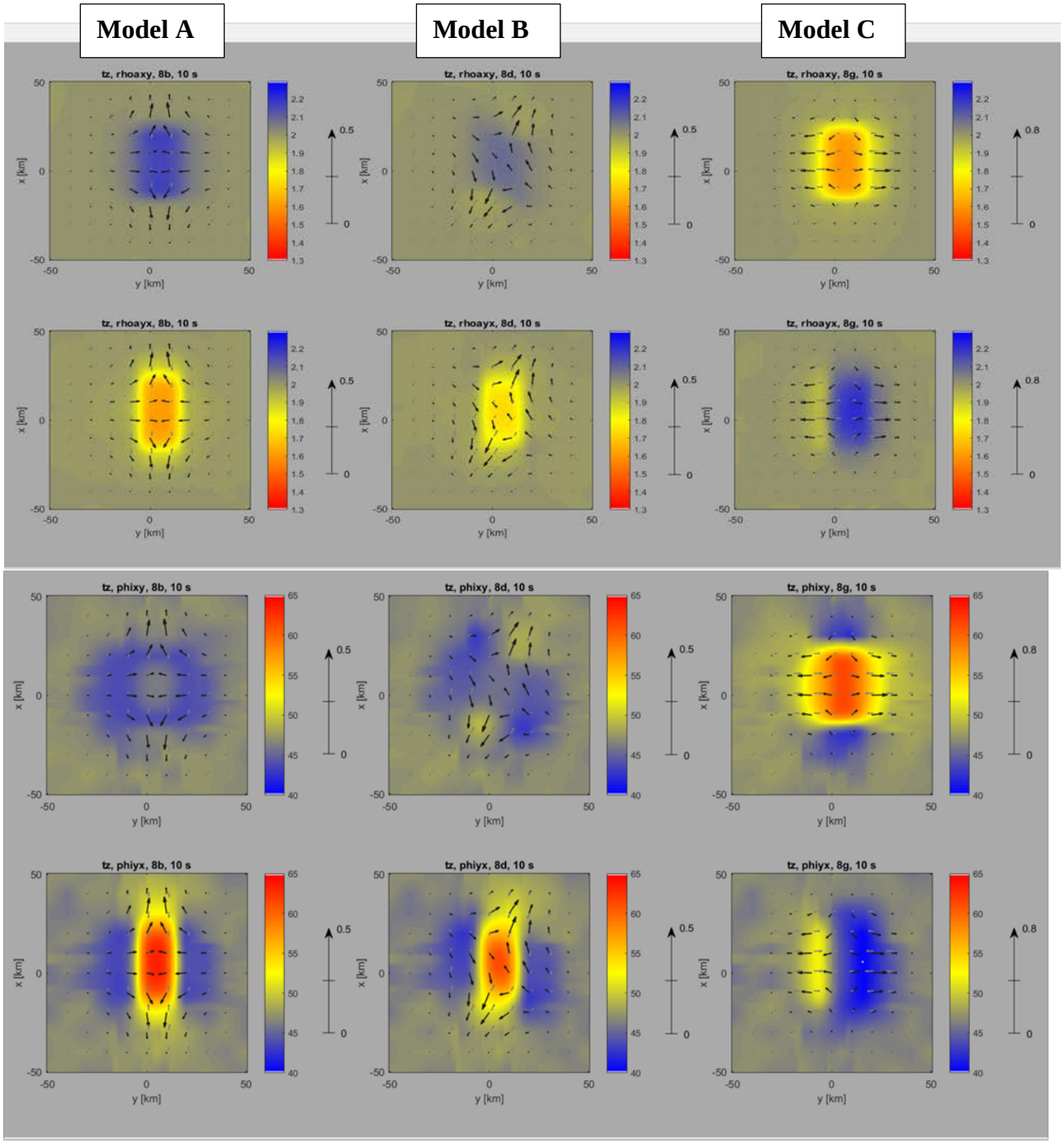

Figure 2. Plane view of MT transfer functions ρ_{xy}(top row), ρ_{yx}(2nd row), φ_{xy}(3rd row), φ_{yx}(bottom row) (colors) and real (black) and imaginary (grey) tipper vectors (Wiese convention) for models A(left), B(center), C(right) (cf Fig. 1 and Tab. 1) for 10s period. Units in $[\Omega m]$and degrees.

RESULTS

Model parameters vary for the resistivity's principal axis values ρ_x, ρ_y, ρ_z and for the Euler angles α, β, γ denoting rotations around the x-, y-, and z-axis. Fig. 2 shows exemplarily results for 3 different parameter sets according to Tab. 1.

Table 1. Parameters for models A,B,C; principal axis values ρ_x, ρ_y, ρ_z in $[\Omega m]$, Euler angles α, β, γ in [°]

model	ρ_x	ρ_y	ρ_z	α	β	γ
A	10	1000	100	0	0	0
B	10	1000	100	0	0	30
C	10	10	1000	60	0	0

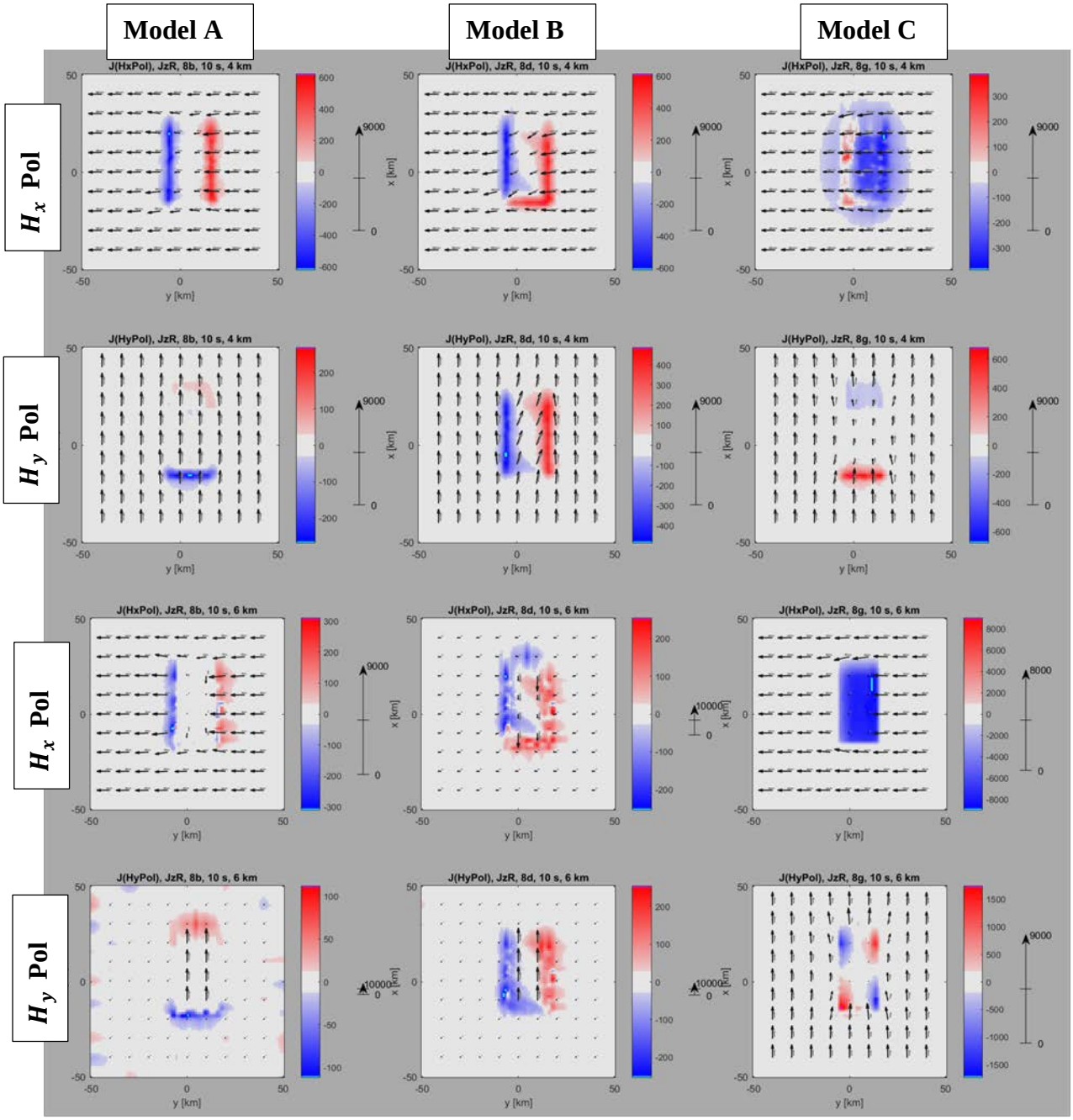

Figure 3. Plane view of current density (arrows (J_x, J_y), $\Re$ black, $\Im$ grey, colours $\Re J_z$) for models A (left), B (middle), C (right) (cf Fig. 1 and Tab. 1) at 4 km (top two rows) and 6 km (bottom two rows) depth for 10s period and H_x and H_y source field polarization (upper and lower row resp.). All quantities normalized units.

The first two rows show the apparent resistivity ρ_{xy} and ρ_{yx} on the surface plane above the anomaly (Fig.1) for a 10 s period. For model A the pattern reflects the TE and TM mode behavior (diffusive resp. sharp transition) at the opposite sides of the anomaly according to the orientation of the magnetic resp. electric field and depending on the direction of the higher and lower resistivity compared to the background resistivity. The corresponding patterns for the phases at the bottom two rows very impressively demonstrate the effect of the highly conducting anomaly in x-direction compared to that of the resistive direction. Additionally, the tipper vectors (Wiese convention) are plotted at 10 km spacing. Pointing towards or away from the anomaly they reflect the lateral resistivity transition at the boundaries resp. the lateral change of the horizontal current density according to the anisotropic resistivity.

For model B the azimuth of the anisotropy is rotated clockwise by 30° compared to model A. As demonstrated

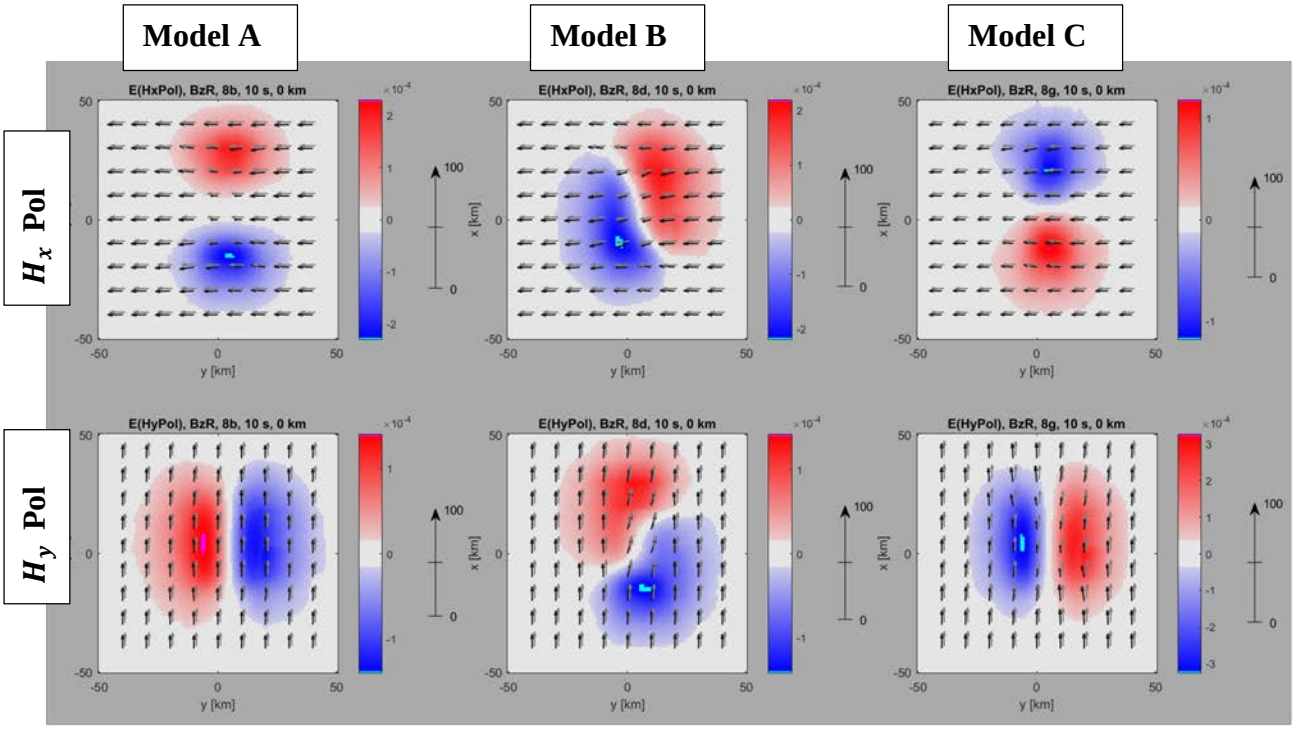

Figure 4. Plane view of surface electric field (E_x, E_y) (arrows, $\Re$ black, $\Im$ grey) andt the vertical magnetic field component $\Re B_z$ (colours) for models A (left), B (middle), C (right) (cf Fig. 1 and Tab. 1) for 10s period and H_x and H_y source field polarization (upper and lower row resp.). All quantities in normalized units.

by Löwer and Junge (2016), the pattern for rhoa and phase values is rotated accordingly, however the tipper vectors take orientations parallel to the anomaly boundary which would not happen for the isotropic case.

In Model C the asymmetric pattern occurs for the H_x polarization due the y direction of the dip.

Fig. 3 shows the current density 1 km above and 1 km below the upper surface of the anomaly for the same situation as in Fig. 2. Note that within the anomaly the current density is decreased resp. increased depending on the source field polarization. Their direction is parallel to the anomaly's boundaries due to electric charges at the boundaries. For model B the currents above the anomaly are also influenced by the charges and they rotate away from the conductive direction of the anomaly. The distribution of the real part of the vertical current density nicely demonstrates how the currents are drawn into the anomaly for its conductive direction resp. deflected around the anomaly for its resistive direction. In model C the dipping anisotropy shows a very different current pattern for the two polarizations caused by the direction of the dip.

At the surface above the anomaly the horizontal magnetic field is obviously less affected than the electric field, which is plotted together with the real part of the vertical magnetic field component in Fig. 4. The deflection is clearly demonstrated for model B, especially for the H_y polarization. Also note that partly the direction of the imaginary part is oblique to that of the real part resulting in an elliptical polarization of the electric field. It seems that the electric field behavior is mostly responsible for the pattern of the apparent resistivity and phase, whereas the deflection of the electric current above the anomaly is related to the asymmetry of the vertical magnetic field component. The appearance of the phase tensor and its relation to the field components within the subsurface will be demonstrated during the workshop.

REFERENCES

Löwer, A., Junge, A., 2017, Magnetotelluric Transfer Functions: Phase Tensor and Tipper Vector above Anisotropic Three-Dimensional Conductivity Anomaly and Implications for 3D Isotropic Inversion, PAGEOPH, in press, 2017